Bulletin of Earthquake Engineering (2023) 21:4065–4089
https://doi.org/10.1007/s10518-023-01660-8

S.I. : GEOTECHNICAL SEISMIC ISOLATION

SAP-sand mixtures as a geotechnical seismic isolation technology: from the dynamic characterization to a simple analytical design approach

Fausto Somma[1] · **Alessandro Flora**[1]

Received: 4 August 2022 / Accepted: 23 February 2023 / Published online: 3 March 2023

Abstract
Seismic isolation techniques are hardly implementable on existing historic structures, if their integrity is a matter of concern (Viggiani in 19th International conference on soil mechanics and geotechnical engineering, Seoul Korea, 2017; Flora in Third international symposium on geotechnical engineering for the preservation of monuments and historic sites, Naples, Italy, 2022). Recent results have shown that if a continuous barrier having a low dynamic impedance is created in the soil beneath the structure, both the absolute acceleration and relative displacement demands are significantly reduced without any direct intervention on the structure itself. Super Absorbent Polymers (SAP), mixed with the in-situ soil, are excellent candidates to the creation of these soft barriers. The first part of the paper reports a complete dynamic laboratory characterization of SAP-sand mixtures with different percentages of polymer in the soil. The results clearly show that small percentages of SAP have a minor effect on the reduction of the shear stiffness value, while when the percentage is higher than 40% a sharp drop is observed. It is also shown that SAP largely increases the damping ratio of the treated layer, being this an extremely beneficial effect for its seismically isolating application. In the second part of the paper, one and two-dimensional seismic response analyses were carried out to explore the beneficial effects of SAP-soil filtering barriers as parts of a Geotechnical Seismic Isolation (GSI) system. The paper also proposes a simplified analytical approach to design geotechnical seismic isolation using Super Absorbent Polymers.

Keywords Geotechnical seismic isolation · Super absorbing polymer · Soft soil · Soft anti-seismic barrier · Soft caisson · Filtering effects

✉ Fausto Somma
fausto.somma@unina.it

Alessandro Flora
flora@unina.it

[1] Department of Structures for Engineering and Architecture, University of Naples Federico II, Via Claudio 21, 80125 Naples, Italy

1 Introduction

An alternative to the classical methods of structural seismic isolation is the reduction of the seismic demand through interventions on the foundation soil. Since seismic demand depends, among other factors, on the deformability of the soil underlying the structure, an artificial modification of the mechanical properties of this part of the subsoil may properly modify the seismic structural demand. The idea of modifying the soil to create a seismic isolation system within the ground is often called "*Geotechnical Seismic Isolation*" (GSI). Such a kind of technique has attracted the attention of many researchers over the years. For instance, the insertion of a sliding surface beneath the structure, with a very low friction angle, significantly reduces the seismic actions on the structure (e.g. Yegian and Catan 2004; Yegian and Kadakal 2004). Alternatively, the creation of a layer of a mixture of rubber chips and soil under the structure to be seismically isolated has been also studied with numerical modelling (Pitilakis et al. 2015; Tsang and Pitilakis 2019; Pitilakis et al. 2021), reduced scale shaking table testing (Xiong and Li 2013) and full-scale field testing (Mahdavisefat et al. 2018). Nowadays, due to their high shear deformability and purely elastic behaviour, the rubber-soil mixtures prove to be one of the most effective geotechnical seismic isolation techniques. Alternately, Somma et al. (2021) proposed to remove the soil on the sides of the embedded shallow foundation to reduce the rotational and translational soil-foundation stiffnesses and, by so doing, to increase the natural period of the structure. The seismic demand reduction, generated by the lateral disconnection, has been validated through geotechnical centrifuge experiments (Somma et al. 2022a). The results of these centrifuge tests were replicated numerically confirming the efficiency of lateral disconnection (Somma et al. 2022b). The beneficial and possible detrimental effects of lateral disconnection were also highlighted with three-dimensional numerical FEM analysis for a building of historical character, namely tower No. 19 of the ancient Constantinople walls (Somma et al. 2023). Furthermore, this last method was analysed by Tsang (2022), introducing the possibility to use an analytical formulation to estimate the effects of the lateral disconnection and to combine this technique with other GSI ideas. Some kinds of GSI ideas consist of injecting materials into the ground able to drastically modified the properties of the soil in terms of stiffness and damping. To this aim, Gatto et al. (2021) recently proposed an effective GSI system based on the injection of expandable polyurethane into the soil through small holes in the slab. One of GSI's oldest and most famous idea is the use of soft or stiff anti-seismic thin barriers in the ground. This idea was first investigated by Kirtas and Pitilakis (2009), Kirtas et al. (2009) and later considered by other authors. Nappa et al. (2016) and Flora et al. (2018) focused their attention on soft buried barriers having different geometrical schemes, analysing their behaviour through centrifuge tests and numerical modelling (Fig. 1a). The most effective anti-seismically scheme consists in the creation of a lower horizontal layer having reduced shear stiffness and four lateral vertical barriers having reduced bulk stiffness (Fig. 1b). In such a way, the bounded mass of soil may be added to that of the foundation, contributing along with the reduced stiffness of the bounding soft barrier to the elongation of the structural period. This geometrical configuration of the SAP-soil layers is called "*soft caisson*". Among other possible technologies, the use of Super Absorbent Polymers (SAP) for the creation of the base soft layer is attractive. SAP is a granular material whose grains have the capacity of retaining huge amounts of water, transforming into highly deformable gelly balls upon hydration (Fig. 2). Different kinds of SAP exist, depending on the use for which they are conceived. In fact, their capacity to absorb and retain water can be engineered. Being environmentally friendly, for

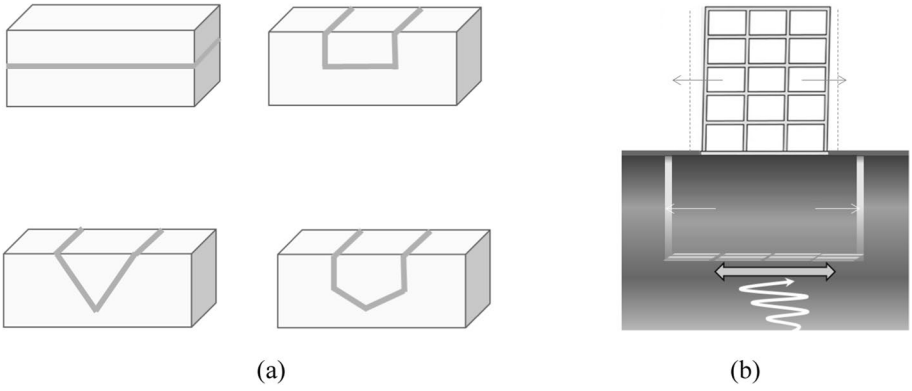

Fig. 1 Geotechnical Seismic Isolation schemes using soft barriers: **a** different geometric layouts; **b** Schematic view of the layout with a base horizontal layer and lateral vertical ones (soft caisson)

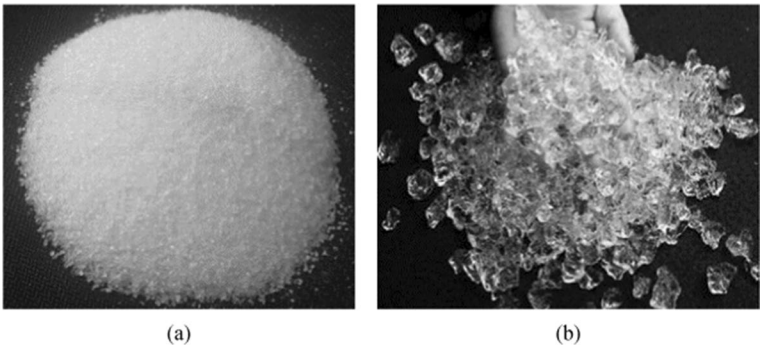

Fig. 2 Super absorbing polymer: **a** SAP in the dry/powder state; **b** hydrated SAP

instance, they are often used in agriculture to slowly release water. In the application considered in this research (and only in the case of applications over the ground water level), SAP has to be engineered to release water at the slowest possible rate, in order to keep for the longest possible time its peculiar jelly-like behavior, that implies an extremely low shear stiffness (in the extreme case of a 100% SAP assembly, the mechanical behavior tends to that of water, and thus the shear stiffness reduces to extremely low values). However, through the use of grouting technology, it is possible to perform the rehydration in site, thus making the engineering use of this material feasible and reliable. Furthermore, in order to control the effectiveness of the soft barriers over time, it is possible to carried out geophysical surveys (MASW, HVSR) or seismic borehole (Cross Hole, Down Hole) tests, capable of highlighting areas with significant shear wave velocity reduction.

This paper will describe the geotechnical seismic isolation through the use of soft barriers made by SAP. The first part of this work focuses on dynamic characterization of SAP-sand mixtures, through laboratory tests. Due to the low shear stiffness of the sand-SAP mixture, the shear strains developed in the soft barrier during a seismic event are expected to be very high. For this reason, the dynamic characterization of these mixtures was carried out in a wide strain range: at very small strain levels, shear stiffness was explored with bender elements (BE) under isotropic confining conditions; at high or very high shear

strain levels cyclic simple shear (CSS) tests were used to investigate the non-linear behavior of the analyzed mixtures. The shear modulus reduction and damping curves have been identified for different percentages of SAP in the SAP-sand mixtures, considering also the reference case of pure sand (i.e. SAP = 0%), which was investigated with resonant column torsional shear (*RCTS*) equipment.

In the second part of this paper, one and two-dimensional numerical analyses will be performed. Since previously published numerical analyses (Flora et al. 2018) were carried out in the hypothesis of a linearly elastic behavior of the soft barriers with no damping, it is expected that the new experimental results presented in this paper will allow the use of more calibrated material models and therefore more refined analyses, thus leading to more realistic predictions of GSI systems created with SAP-sand mixtures. In particular, in the two-dimensional FEM analysis, the importance of the natural periods of vibration of the soft caisson will be outlined. In order to show the dynamic behavior of the soft caisson and to have a preliminary design tool, a two degree of freedom dynamic system is also presented. This tool will help to find the best solution of the soft caisson dimension and properties case by case.

2 Material characteristics and specimen preparation

The sand used in this study is Hostun HN31 sand, with specific gravity $G_s = 2.65$, maximum and minimum void ratio $e_{max} = 1.011$ and $e_{min} = 0.555$, and critical state friction angle $\varphi_{cv} = 33°$ (Flavigny et al. 1990; Heron 2013). The Hostun Sand is made by high siliceous amount ($SiO_2 > 98\%$) and, as it is possible to see by optical microscope image, the grain shape varies from angular to sub-angular (Fig. 3a) The grain size distribution (Fig. 3b) confirms that it is a medium-fine sand with a uniformity coefficient (Cu) equal to 1.3. As previously shortly mentioned, SAP is a synthetic powder material. The one used in this research is a polyacrylic acid partial sodium salt (see: http://www.sigmaaldrich.com/catalog/product/aldrich/436364?lang=it&region=IT). This superabsorbent is composed of crosslinked networks of hydrophilic polymers able to absorb distilled water up to 240 times (1:240) its own initial weight.

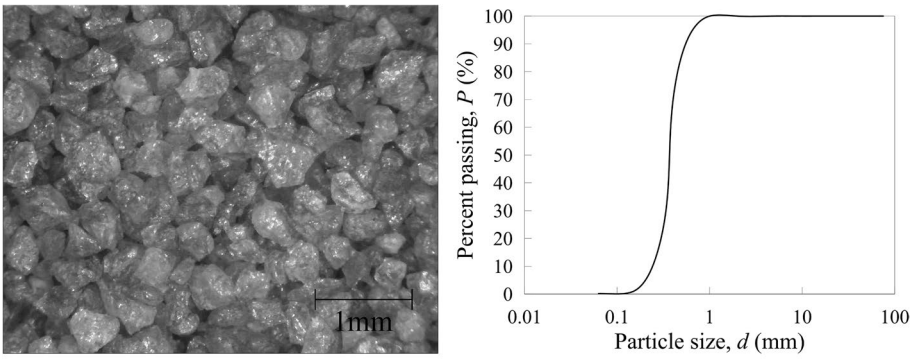

Fig. 3 Physical properties of Hostun Sand: **a** picture with an optical microscope; **b** grain size distribution

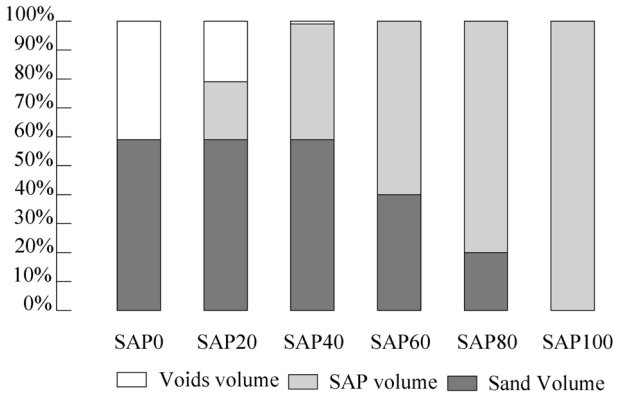

Fig. 4 Scheme of theoretical volume percentage of SAP for each studied specimen

Table 1 Summary of tests carried out on different SAP-sand mixtures

SAP-sand mixture	% SAP by volume (%)	B.E. tests	C.S.S. tests	R.C. test
Sand	0	•		•
SAP40	40	•	•	
SAP60	60	•	•	
SAP80	80	•	•	
SAP100	100	•		

The effect of mixing sand and SAP largely depends on the relative amounts. For low percentages of SAP, its grains tend not to become part of the micromechanical structure of mixture, and can be seen as essentially filling the existing voids (Flora et al. 2015). Because of this, when in low percentages, SAP can be expected to have a minor effect on shear stiffness (linked to a possible increase of void ratio). Theoretically, the maximum volume of SAP to be added to have the above-mentioned behavior (i.e. only filling the voids) is equal to the volume of the voids themselves. Likely, it will be a lower volume, as it is physically impossible that the SAP particles arrange in this very peculiar pattern.

For higher fractions of SAP, its grains inevitably take part to the mixture microstructure, thus modifying significantly the stress chains properties. As a consequence, a much more relevant effect is expected in terms of shear stiffness decrease and damping ratio increase.

The relative density selected in this study for the sand is $D_r = 0.7$, corresponding in this case to a void ratio $e = 0.69$. Figure 4 summarizes the different theoretical compositions of the SAP-sand mixtures studied in this work, where SAPXX indicates the percentage of SAP by volume with respect to the total volume. The actual SAP percentage by volume of the realized samples differs by a maximum of 2% from the theoretical design percentage. For this reason, the outlined difference does not affect the reliability of the results.

Table 1 summarizes the dynamic tests carried out for each SAP-sand mixture. In particular, BE tests were carried out at confining pressures of 10, 55, 150 kPa, while CSS tests were carried out only for a confining stress of 55 kPa. Furthermore, due to the particular difficulty in sample preparation and massive load head of the *RCTS*, it was only possible to perform *RCTS* test in the case of pure sand with 55 kPa of confining stress. In order to

understand the influence of the hydration percentage of SAP on dynamic mixture properties, the BE test at 55 kPa of confining pressure was carried out twice, once using a hydration ratio of 1:150 (smaller SAP grains) and once of 1:240 (bigger SAP grains). In all the other cases the SAP hydration ratio was fixed to 1:150.

3 Laboratory investigation

3.1 Bender element (BE) tests

The bender element tests were carried out in a conventional triaxial cell (Fig. 5). The travel time ($t_{c.c}$) of the shear waves in the specimen was obtained by using a Cross Correlation (*C.C.*) procedure (Viggiani and Atkinson 1995) between the transmitter (input) and the receiver (output) signal track considering the transverse directivity (Lee and Santamarina 2005). Figure 6a shows the input and output signal traces as the input frequency changes with 1:240 hydrated SAP, while in Fig. 6b the SAP was hydrated at 1:150; in both cases, an isotropic confining pressure of 55 kPa was applied. As expected, the higher the percentage of SAP, the lower the shear wave velocity in the sample. Interpreting the results of all *BE* tests, the value of shear waves velocity could be expressed as a function of the SAP percentage in the specimen (Fig. 7). Using non-linear least square method, the following best fitting correlation results in this case:

$$V_s = V_{s,0} * \frac{1}{1 + \left(\frac{SAP\%}{A}\right)^B} \tag{1}$$

where $V_{s,0}$ is the shear waves velocity of the pure sand, at the considered confining pressure, *SAP%* is the volume percentage of SAP in the mixture, A and B are non-dimensional coefficients that depend on the effective confining cell pressure. In order to show the fitting efficiency, Fig. 7 also shows the low values of the residual standard deviation, *RSD*, calculated as follows:

Fig. 5 Bender element triaxial cell used

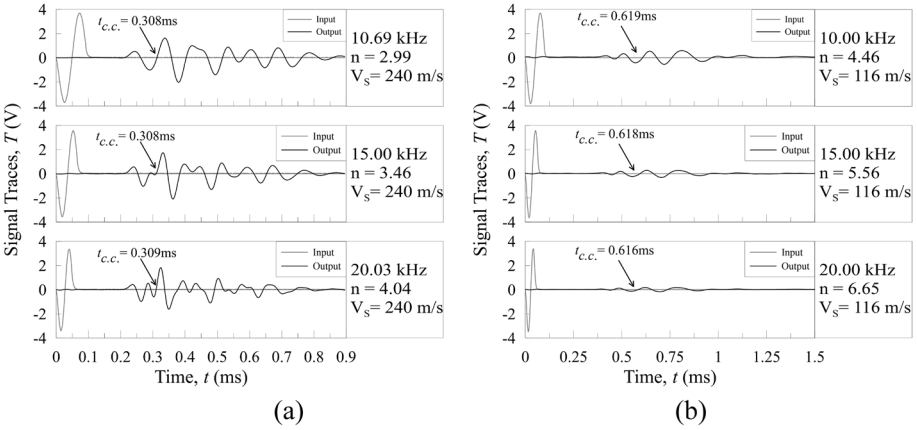

Fig. 6 Input and output signal track at a confining pressure of 55 kPa with indication of the input frequency, $n = \frac{L}{\lambda}$ and V_s: **a** SAP hydration ratio equal to 1:240 **b** SAP hydration ratio equal to 1:150

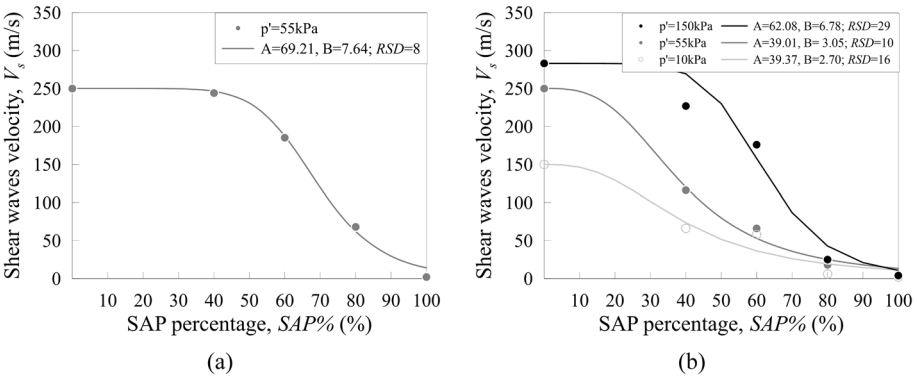

Fig. 7 Shear waves velocity reduction as function of the SAP percentage: **a** Confining pressure equal to 55 kPa, and hydration ratio 1:240; **b** Confining pressure equal to 10, 55, 150 kPa and hydration ratio 1:150

$$RSD = \sqrt{\frac{\left(Y_i - \hat{Y}_i\right)^2}{n-2}}$$

where Y_i is the experimental value while $\hat{Y}_i$ is the predicted value and n is the sample size.

In particular, Fig. 7a shows the shear waves velocity reduction as a function of the SAP percentage at 55 kPa of confining pressure with SAP hydration ratio equal to 1:240, while Fig. 7b shows the different value of V_s at 10, 55, 150 kPa of confining pressure with hydration ratio equal to 1:150. The results clearly highlight the role of SAP in reducing the shear stiffness of the mixture.

Especially for high SAP content (> 60%), the reduction of the shear wave velocity is very high (> 70% on average). Comparing the curves regarding differently hydrated SAP (1: 240–1: 150), at a confinement pressure of 55 kPa, it is also possible to see a different

behavior of the shear waves velocity reduction curve. In particular, for a less hydrated SAP (1:150), at SAP percentage of 40%, the shear waves velocity has already significantly decreased, while for the mixture with more hydrated SAP (1:240) and the same percentage, it is still almost equal to that of clean sand. This can be explained, from a micromechanical point of view, by considering that a more hydrated SAP, with the same overall volume of polymer introduced into the soil, is made by a lower number of bigger particles, thus resulting in a less homogeneous micromechanical fabric; conversely, a less hydrated SAP will have smaller and more uniformly diffused particles within the soil. In this latter case, therefore, the SAP particles will likely be able to break the shear stress chains more effectively. Even though this effect of hydration is general, its quantitative effect is strictly related to the kind of SAP and sand used, and thus cannot be generalized. Figure 8 reports a schematic representation of this micromechanical interpretation. As already mentioned, the non-dimensional coefficients A and B depend on the confinement pressure. By evaluating these coefficients for three different confining pressures, the following best fitting general expressions (residual standard deviation, *RSD*, almost equal to zero) of A and B as functions of the mean effective stress, *p'*, are herein proposed:

$$A = 40.4 - 12.4\left(\frac{p'}{p_{ref}}\right) + 17.9\left(\frac{p'}{p_{ref}}\right)^2 \tag{2}$$

$$B = 2.74 - 0.68\left(\frac{p'}{p_{ref}}\right) + 2.25\left(\frac{p'}{p_{ref}}\right)^2 \tag{3}$$

where p_{ref} is equal to 100 kPa.

3.2 Resonant column torsional shear test

A resonant column torsional shear test was carried out to obtain the variation of the normalized shear modulus, G/G_0, and the damping ratio, ξ, with shear strain, γ, required to characterize the non-linear behaviour of the pure clean sand. Figure 9a and b show, respectively,

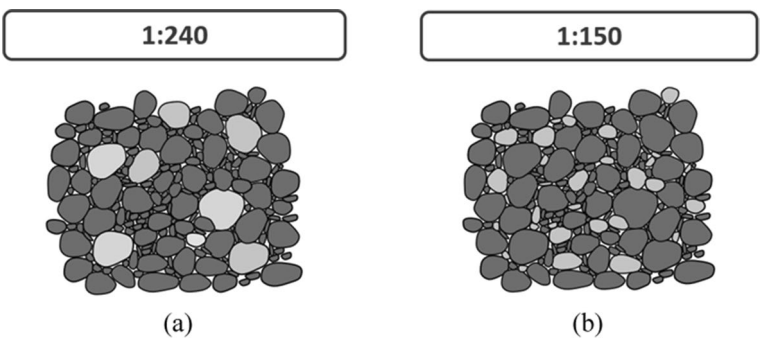

Fig. 8 Schematic drawing of the SAP-soil mixture with different hydration ratios at the same overall percentage: **a** high hydration raio (1:240) with SAP particles as isolated inclusions; **b** low hydration ratio (1:150) with SAP particles more homogeneously distributed within the mixture mass

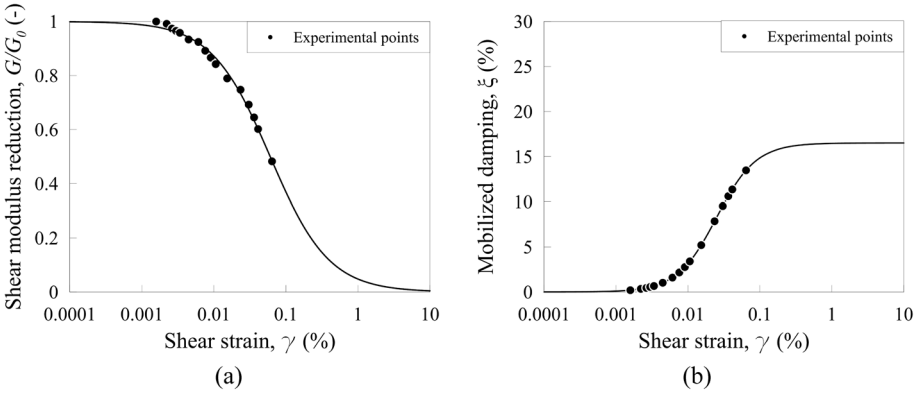

Fig. 9 Experimental results of the RC test on clean Hostun Sand: **a** shear modulus reduction curve; **b** mobilized damping curve

the normalized shear modulus and the damping experimental points of the pure clean Hostun sand, analytically fitted by the MKZ model (Matasovic and Vucetic 1993).

3.3 Modified NGI simple cyclic shear test

Three modified NGI cyclic simple shear tests (Bjerrum and Landva 1966), in constant volume drained conditions (Airey and Wood 1986), were performed on different SAP-sand mixtures (Table 1). The tests were performed in strain-controlled mode and the investigated range of shear deformation goes from around 0.1% to 10% of the initial specimen height. For each level of deformation, 5 shear cycles, at 1 Hz frequency, were applied. This is the highest possible frequency in the used simple shear device, and was adopted being close to the typical range of the main frequencies of earthquakes (which usually lies between 1 to 2 Hz). Figure 10 shows the non-linear hysteretic loops for different SAP-sand mixtures presented in Table 1, increasing the amplitude of the shear strains. As typical, the secant shear modulus was calculated using Eq. 4:

$$G_{sec} = \tau_{pp}/\gamma_{pp} \tag{4}$$

where τ_{pp} is the peak to peak stress value and γ_{pp} the peak to peak strain value in each cycle. The evaluation of the damping mobilized with shear strain is influenced by the loop asymmetry and, for this reason, different procedures were adopted to compute the experimental damping points (Fig. 11). In particular, due to the asymmetric nature of the shear-strain cycles, the procedure proposed by Kumar et al. 2018 and the one indicated by the modified ASTM (ASTM D5311) have been adopted. Figure 12 shows the damping values obtained using these two procedures, analytically fitted by the MKZ model. The damping values found trough Kumar et al.'s procedure are generally lower than those found via the modified ASTM procedure (−15% on average), with differences that increase with the increase in SAP percentage. This is due to the different method used to compute the elastic energy introduced in the system. Considering that damping accounts for the hysteretic dissipation of energy and is therefore a beneficial material property to reduce seismic actions,

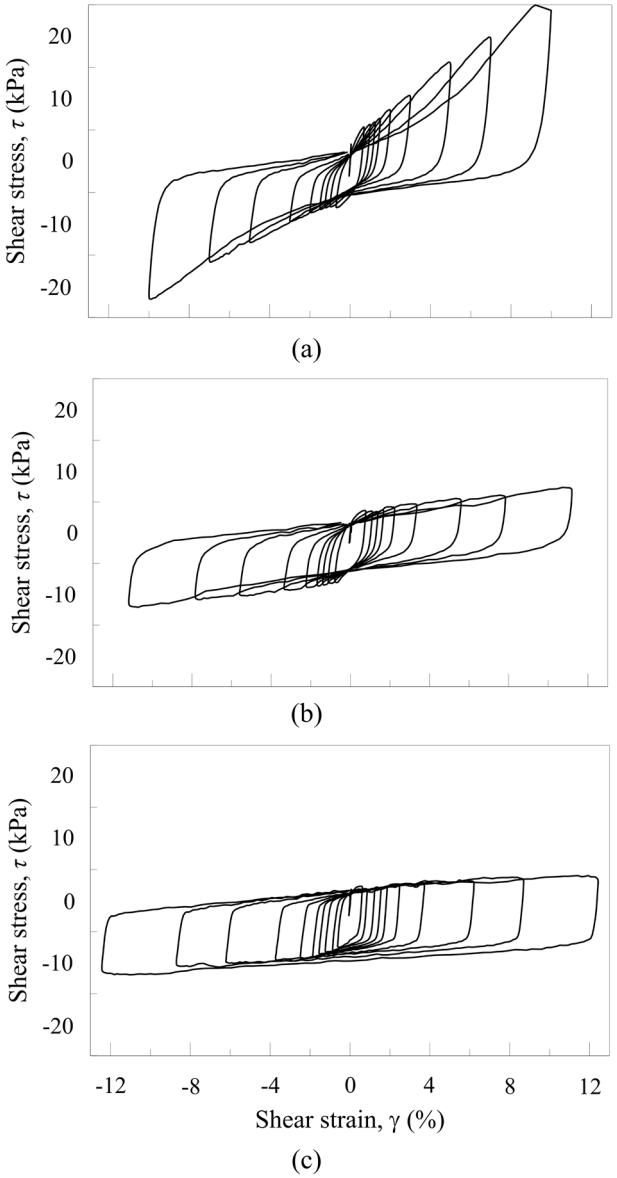

Fig. 10 Experimental stress–strain loop found through the CSS tests for different SAP-sand mixtures: **a** SAP40; **b** SAP60; **c** SAP80

it can be concluded that the procedure proposed by Kumar leads to a conservative estimate of the damping values.

It is also extremely interesting to highlight that, at the high shear strain levels expected in SAP-sand mixtures during seismic actions, extremely high values of damping are mobilized, confirming the attitude of SAP-sand mixtures to be used in geotechnical seismic isolating (GSI) systems. In fact, the mobilized damping increases from around 5% at medium

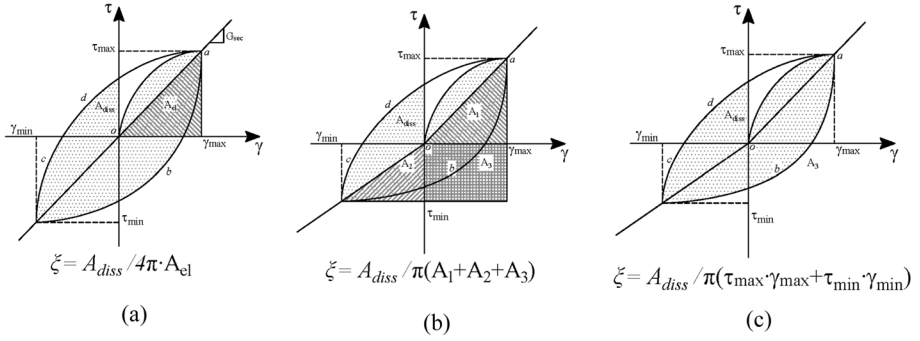

Fig. 11 Different procedure to compute the damping mobilized with shear strain: **a** Classical ASTM method for symmetric shear strain loop; **b** Formulation proposed by Kumar et al. (2018) for asymmetric loops; **c** Modified ASTM method for asymmetric loops

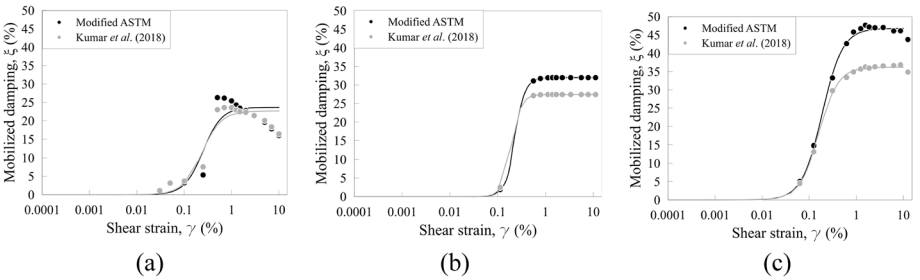

Fig. 12 Damping curves for different SAP-sand mixtures: **a** SAP40; **b** SAP60; **c** SAP80

shear strain range (0.1%) to 25, 35, 45% at a high shear strain range (> 1%), respectively for SAP40, SAP60, SAP80. The maximum sand damping value is tripled using the SAP80 mixture, while it is doubled in the case of the SAP60 mixture. By combining the results of the BE tests (conventionally assumed to be related to a mobilized value of the shear strain $\gamma = 0.0001\%$) with those of the C.S.S. tests, it is then possible to find the decay curve of the shear modulus for the different studied mixtures (Fig. 13). As it possible to see, the addition of the jelly particles of SAP increases the linear range, which stretches to the high value of $\gamma \approx 0.1\%$ for the SAP80 mixture.

4 Numerical analysis

4.1 One dimensional analysis

In order to highlight the beneficial effect of anti-seismic soft barriers, a series of one-dimensional seismic response analyses were carried out by varying the sand-SAP properties (i.e. considering different relative percentages of the two components) and the depth of the soft layer in the ground. A visco-elastic non-linear equivalent model was used by means of the code STRATA (Kottke et al. 2019). The depth of the deformable soil is fixed at 30 m. The bedrock has been modelled as a visco-elastic half space with a damping ratio

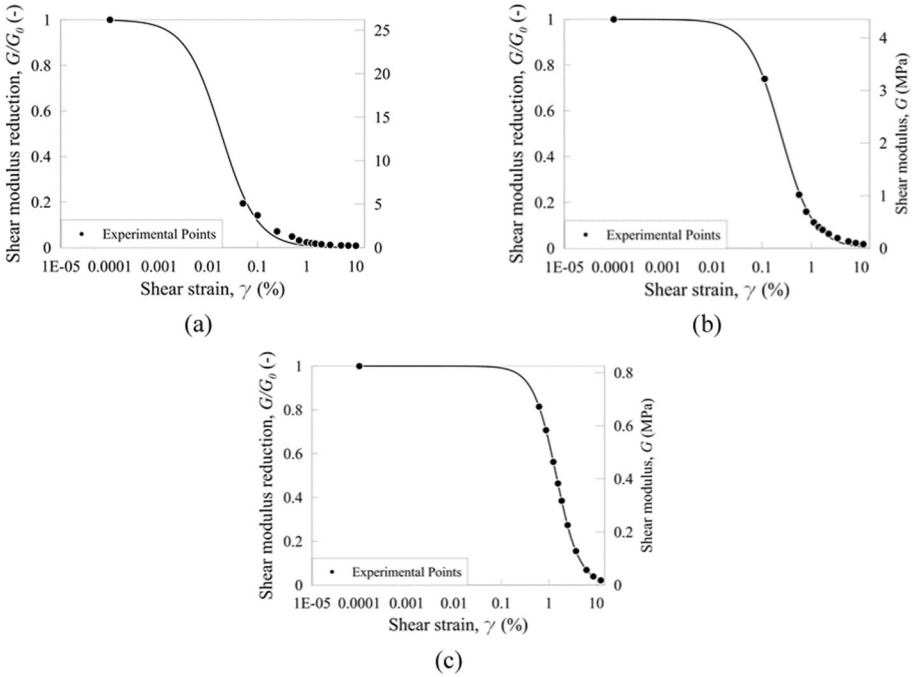

Fig. 13 Shear modulus reduction curves obtained combining the BE tests and CSS test: **a** SAP40; **b** SAP60; **c** SAP80

of 0.5%. Small strain shear stiffness was modelled using the formulation suggested by Hardin and Drnevich (1972):

$$G_0 = A \bullet \frac{(2.17 - e)^2}{1 + e} \bullet \left(\frac{p'}{p_{ref}} \right)^m \tag{5}$$

The parameters of Eq. 5 were calibrated on the results obtained on Hostun Sand by Hoque and Tatsuoka (2000) at a relative density of 70%: A =80, m =0.47, e =0.692 and p_{ref}=100 kPa. The increasing stiffness profile with depth was simulated, in the numerical model, by discretizing the soil layers meter by meter. A barrier of SAP-sand mixture (considering the two cases SAP60 and SAP80) having a thickness of 1 m was placed at different depths (5, 10, 15, 20 m). The shear wave velocity in the SAP-sand mixtures was evaluated using Eq. 1, considering the influence of the mean pressure at the specific depth where the mixture was placed. The estimated non-linear properties found through the aforementioned laboratory tests, $G/G_0(\gamma)$ and $\xi(\gamma)$, of both Hostun sand and SAP-sand mixtures, were assigned in the numerical model. A series of spectra compatible earthquakes, on soil class type A (rock), were selected and applied at the base of the numerical model, considering the specific seismic hazard of the city of L'Aquila (Italy) at the life safety limit state with return period, T_r, equal to 475 years (as defined by the Italian building code, IBC (2018) (Fig. 14). Table 2 reports the main dynamic features of the selected earthquakes. The anti-seismic effectiveness of the soft layers is analyzed comparing the dynamic behavior of the soil bank with and without the soft barrier. The case in which the soft SAP-sand barrier is introduced is referred to by the acronym GSI (Geotechnical Seismic Isolation). Three

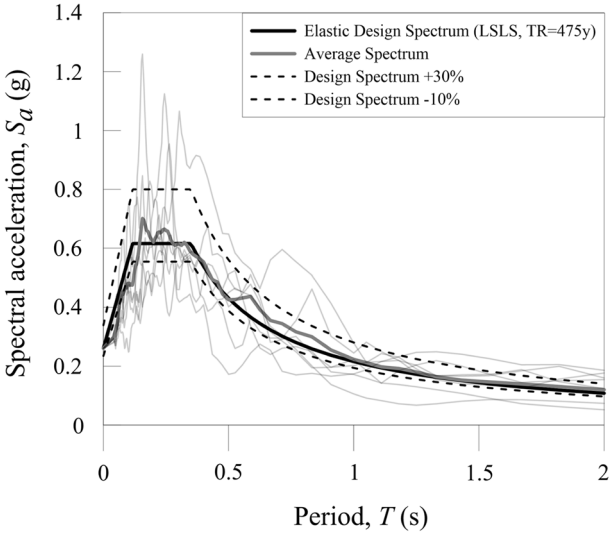

Fig. 14 Compatibility spectrum analysis related to the life safety limit state elastic spectrum for the city of L'Aquila (Italy), following the Italian building code (NTC2018)

Table 2 Characteristics of the earthquakes used in the parametric analysis

Location	T_d (s)	T_m (s)	I_A (m/s)	$T_{5\text{-}95}$ (s)
Bingol	0.16	0.33	0.51	4.56
Campano Lucano	0.10	0.49	1.27	40.33
Friuli	0.26	0.39	0.42	4.3
Golbasi	0.26	0.72	0.50	11.85
Mt. Fnajoll	0.20	0.59	0.40	7.96
South Iceland	0.24	0.47	0.63	4.45
South Iceland After	0.30	0.58	0.89	5.33

different parameters as a metric of anti-seismic efficiency has been selected: *PGA* efficiency, $E_{PGA}=(PGA-PGA_{GSI})/PGA)$, Arias Intensity Efficiency, $E_{IA}=(IA-IA_{GSI})/IA)$ and Housner Intensity Efficiency, $HI=(HI-HI_{GSI})/HI)$. Figure 15 shows the effect of inserting a soft layer characterized by SAP80 at variable depths. The anti-seismic efficiency, up to 15 m of treatment depth, is particularly high, reaching values higher than 0.7 for barriers placed at a depth of 10 m. The scattering of the efficiency values, through different earthquakes, is generated by the various degree of dynamic coupling between the mean frequencies (Rathje et al. 1998) of the input signals and those of the soil bank with and without the soft barriers. In this 1D analysis, starting from 15 m depth of the barriers, the anti-seismic efficiency is considerably reduced. As a matter of fact, with 20 m depth of the barriers, the dynamic impedance contrast between the soil and the soft layer is reduced. For this reason, increasing the depth of the barrier will generate less mobilized damping and shear modulus reduction in the soft layer (Fig. 16). However, this effect is strictly related to the influence of confinement pressure on shear modulus of SAP-sand mixtures used. Indeed, as it is possible to see in Fig. 7b, for different SAP volume content, the dependence between the shear waves velocity and effective stresses differs, reducing significantly for very high SAP contents (> 80%).

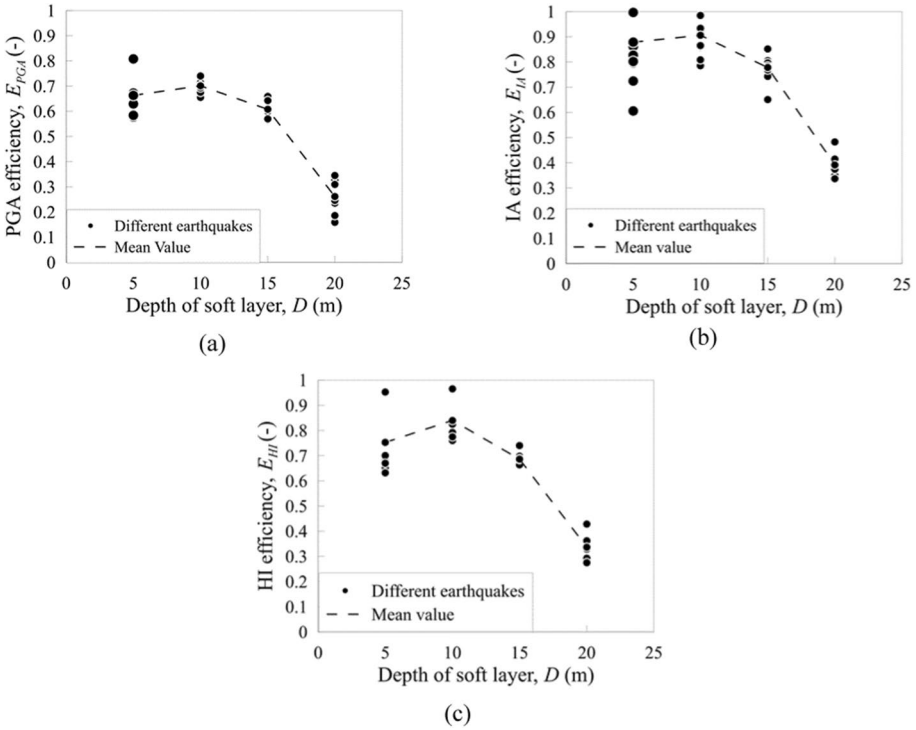

Fig. 15 Efficiency parameters for soft barriers made by SAP80 varying the depth of the soft layer: **a** Peak Ground Acceleration efficiency; **b** Arias Intensity efficiency; **c** Housner Intensity Efficiency

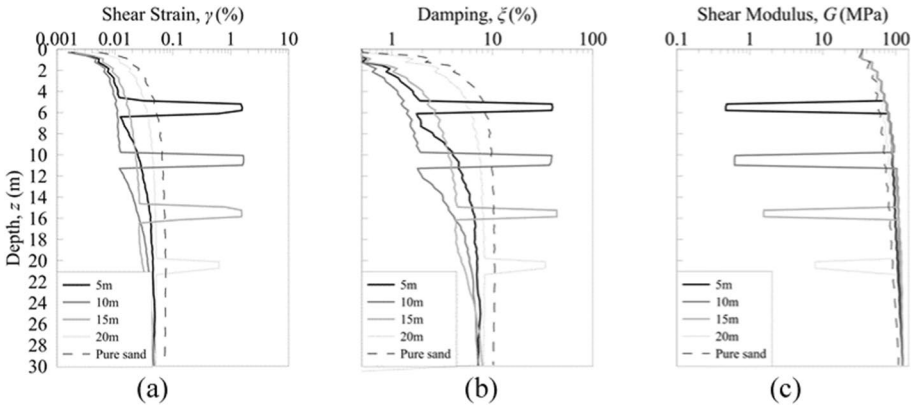

Fig. 16 Different damping and stiffness properties for different depths of the soft layer: **a** Maximum shear strain mobilized as mean of overall earthquakes; **b** Mean damping mobilized in the soil bank; **c** Mean shear modulus mobilized in the soil bank

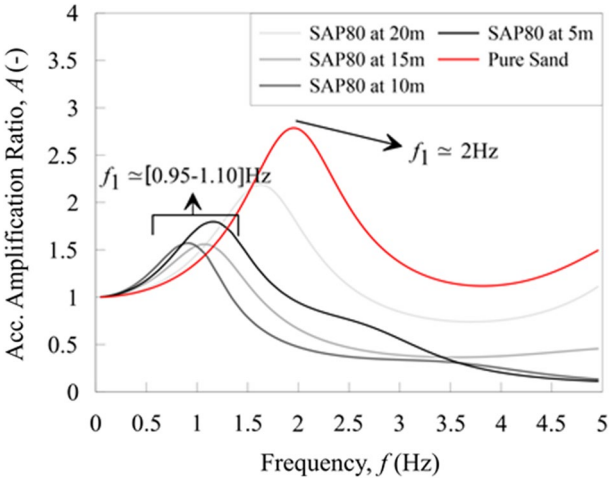

Fig. 17 Effect of the insertion of the soft layer: Acceleration amplification ratio between the top surface and outcrop bedrock signals

The main dynamic effect of inserting a soft layer in the soil is the reduction of the natural fundamental frequency of the soil bank (Fig. 17). The acceleration amplification function, ratio between the Fourier acceleration spectrum at the surface with the one at the outcrop bedrock, shows that the first average fundamental frequency of the soil bank is around 2 Hz, while it is reduced to values even lower than 1 Hz with the soft layers. For this reason, soft barriers can be extremely effective for protecting low-period (squat) buildings, while they can be ineffective or even detrimental for high-period buildings.

4.2 Two-dimensional analysis

Two-dimensional *FEM* analysis with soil-structure interaction were also carried out with Plaxis 2D code (Brinkgreve et al. 2011). With two-dimensional analyses it is possible to study the so called "*soft caisson*" effect. In fact, the presence of an horizontal soft barrier and two vertical barriers (or 4 vertical barriers in three-dimensional view) will generate a completely different dynamic system characterized by its own dynamics properties.

The numerical model with soft barriers (*GSI* model) is shown in Fig. 18 while the benchmark model (*NO GSI* model) is practically the same but without the presence of the soft barriers. The 7 spectrum-compatible accelerograms selected correspond to those used

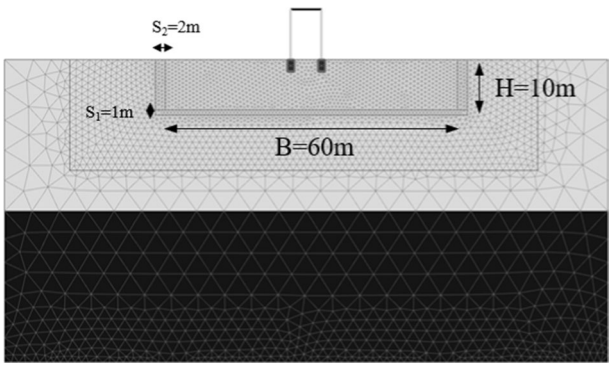

Fig. 18 Two-dimensional numerical model with soft caisson GSI technology

for the one-dimensional analyses (already showed in Table 2 and Fig. 14) while the soil was modelled with Hardening Soil Small Strain (HS_{ss}) (Schanz and Vermeer 1998; Schanz et al. 1999). The selected parameters of the HS_{ss} represent the same soil and same increases in stiffness as in the mono-dimensional analysis (Table 3). The properties of the modelled structure are outlined in Table 4. In particular, the modelled structure wants to represent the standard dynamic properties of masonry building. Regarding the geometrical shape of the SAP in the soil, it was decided to use the rectangular caisson arrangement made by SAP80 with the thickness of the lateral and horizontal barriers equal to two and one meters respectively. The width of the soft caisson (B) is equal to 60 m while the height is equal to 10 m (H). Mohr–Coulomb material constitutive model with operative stiffness and damping values derived from the level of shear deformation achieved in the soft barriers was used (Table 5). The constant volume friction angle of SAP80 ($\varphi'_{cv} = 10°$) comes from direct shear and ring tests (Flora et al. 2015, 2018).

The model has a width dimension of 120 m and a total depth of 60 m. The width of the deformable soil is fixed at 30 m while other 30 m of bedrock are included in the model to ensure no significative interference between the bottom complaint base and the deformable soil layer. The ground water is absent. Standard boundary conditions were applied during the initial (static) stage, that is zero horizontal displacements along the lateral boundaries and fixed nodes at the base of the mesh. During the dynamic analysis, the seismic inputs were applied to the bottom nodes of the mesh. In order to consider the finite stiffness of the underlying bedrock, and to reproduce the upward propagation of shear waves within a semi-infinite domain, the outcrop input accelerations were halved to compute the corresponding upward-propagating wave motion and applied to the bottom nodes together with adsorbing viscous dashpots (complaint base). Free-field boundary conditions were applied along the lateral sides of the mesh. The element size of the soil has been taken always smaller than one-tenth of the wavelength associated with the highest frequency component of the input wave containing appreciable energy (Kuhlemeyer and Lysmer 1973). For this reason, the discretization was carried out using 5933 tetrahedral elements with 15 nodes each. The 30 m relative distance between the lateral barriers and side model boundaries of the models ensures no significant interaction.

The results of two-dimensional analysis confirm the beneficial effects of the SAP; as can be seen from Fig. 19, the presence of the soft barriers drastically modifies the accelerations between the bedrock and the surface. The surface-bedrock acceleration ratios ($a_{max,\ surf}/a_{max,\ bedrock}$) with soft barriers are generally lower than in the pure sand case. The surface-bedrock acceleration ratios are closely related to the mean period of earthquakes. As matter of fact, the closer the earthquake mean period is to resonant period of soft caisson, the more the surface-bedrock acceleration ratio increases. Furthermore, the significant change in frequency content of the seismic signal, generated by the SAP layers, contributes to reduce the resonance phenomena between the seismic signals and the structure.

Indeed, in the design process of soft caisson the estimation of its natural period of vibration is of primary importance. A resonance period of the soft caisson far enough from the earthquake mean period and from the resonance period of the structure will generate large reductions in accelerations. This last aspect is very important and, as will be show clearer in Sect. 5, corresponds to the design strategy of the soft caisson sizes and properties. In order to calculate the caisson natural period of vibration, the acceleration amplification function between the bedrock and the surface of the numerical model can be used. Taking Bingol earthquake as reference, Fig. 20a shows the amplification function with and without the soft barriers. It is worth mentioning that the amplification function without the soft barriers will show the first natural period of the subsoil.

Table 3 Strength and stiffness parameters of sand for numerical analysis with HSss

Soil name (–)	γ (kN/m^3)	c' (kPa)	φ'_{peak} (°)	Ψ (°)	K_0 (–)	G_0^{ref} (MPa)	m (–)	E_{50}^{ref} (MPa)	E_{oed}^{ref} (MPa)	E_{ur}^{ref} (MPa)	$\gamma_{0.7}$ (–)
Hostun Sand	15.37	1	40	10	0.36	128	0.49	35	35	105	0.27E−3

A resonance frequency of the soft box in the range of 1–1.10 Hz (period 0.9–1.0 s) can be estimated whereas, without the soft barriers, the first natural frequency of the soil deposit was approximately equal to 2 Hz. In this case, it can therefore be seen that the soft caisson is able to double the natural period of vibration of the soil bed. This contributes significantly to the reduction of seismic actions on the analysed structure as it moves the resonance frequency of the structure away from the resonance frequency of the soil bed. To better understand this concept, it is possible to calculate the efficiency in terms of the reduction in Pseudo Acceleration at the base of the structure. An efficiency parameter, calculated as $E_{PSA} = (PSA(T)\text{- } PSA_{GSI}(T)/PSA(T)$, will clearly indicate for which values of a single degree of freedom system there will be reductions in maximum acceleration. Figure 20b shows how for structures with a first natural period up to 0.7 s there will be a reduction in acceleration (positive value of E_{PSA}), whereas from 0.7 s onwards the intervention would lead to an increase in the acceleration on the structure, thus being detrimental. This leads to an obvious but essential consideration. The soft barriers technique in the ground is able to protect the generic structure from seismic actions, provided the caisson is adequately designed in its geometry and mechanical properties. Therefore, the application of this technique in engineering practice is suited for low to medium rise structures such as masonry buildings, while it could be detrimental for high period structures such as slender buildings. Again, the effectiveness of the soft barriers has to be analysed case by case.

Different efficiency parameters can be introduced to quantify the benefits of this technique, such as the effectiveness in terms of acceleration reductions ($\eta_a = 1 - (a_{\max,GSI}/a_{\max})$, or Arias Intensity reduction ($\eta_{IA} = 1 - (I_{A,GSI}/I_A)$ of the structure roof (Fig. 21a). Regarding the structural displacement, it is possible to introduce the effectiveness in terms of maximum drift reduction ($\eta_d = 1 - \left(d_{GSI,max}/d_{NOGSI,max}\right)$ (Fig. 21b). The structural drifts are calculated by subtracting from the total horizontal displacement of the roof, both the component due to the rigid global rotation of the structure and the component due to the horizontal displacements at the foundation level.

The effectiveness of the technique is remarkable, in particular for some of the seismic actions considered, contributing to a reduction of up to 45% of the maximum accelerations and of 80% in Arias intensity. In terms of structural displacements, efficiency values reach peaks of 50% for some earthquakes with an average value of 30%. As already stated, the scattering of the efficiency values between the selected earthquakes are mainly due to their different mean frequency contents.

Finally, it is possible to quantify undesirable effects generated by this technique such as high settlements or residual global rotation. Since the horizontal SAP80 barrier has very high volumetric stiffness (Nappa et al. 2016), the total absolute settlements values (δ) as well as the transient maximum structure rigid rotation during the earthquake (β_{max}) and the residual tilt of the structure after the earthquake (β_{res}) are not able to compromise the stability of the structure

Table 4 Properties of the modelled structure adopted in the two-dimensional analyses

Parameter	Prototype
Nominal bearing pressure	95 kPa
Foundations width	1.40 m
Natural frequency (fixed base)	3.33 Hz
Superstructure mass	18.71 Mg/m
Foundation mass	8.44 Mg/m
Base width	7.5 m
Total height	10 m
Geometrical aspect ratio	1.3
Lateral stiffness	8976 kN/m/m
Damping ratio	5%

(Table 6) following the indication of Skempton and Macdonald (1956), Charles and Skinner (2004) for masonry buildings.

5 Two degrees of freedom simplified dynamic system

The soft caisson dynamic system can be studied as a one degree of freedom system moving horizontally under seismic actions. Flora et al. (2018) found that the resonant frequency of a rectangular soft caisson without the presence of the structure can be estimated as:

$$f_{IS} = \frac{1}{2\pi} \bullet \left[\frac{1-\xi^2}{\rho} \left(\frac{2E_g}{S_1 B} + \frac{G_g}{S_2 H} \right) \right]^{0.5} \tag{6}$$

where:

- ρ is the soil density of the isolated volume;
- ξ is the mobilized damping in the barriers;
- E_g is the normal stiffness of the vertical barriers; in particular E_g refers to the compressive stiffness, that may be the oedometer one if the ratio *B/S* is high and confinement is provided, or the Young modulus in all other cases;
- G_g is the shear stiffness of the horizontal barrier;
- S_1 and S_2 are the thickness of the lower and side barriers respectively

In order to consider the structure on top of the isolated mass, a possible upgrade of Eq. 6 can be introduced. Indeed, the new dynamic system (soft caisson + structure) can be modelled as two lumped masses in series (Fig. 22). The DDOF (Double Degree of Freedom system) is characterized by:

1. The mass of the soil plus the mass of the foundation (mass A), that move together and provide the input to the superstructure mass. It is therefore assumed that the isolated soil and the foundation vibrate in phase, as SSI ground-foundation stiffness will be much greater than that of the soft material.
2. The top-structure mass (mass B), that moves due to the movement of the lower, isolated mass (mass A)

Table 5 Stiffness and strength parameters for the soft barriers in the FEM numerical analysis

Density of SAP80, p (kg/m^3)	Shear modulus of horizontal barrier, G_g (kN/m^2)	Young modulus of vertical barriers, E_g (kN/m^2)	Friction angle of SAP80, φ'_{cv} (°)
1319	581	1512	10

The spring overall stiffness (k_{barr}) for the soil-caisson system, is the sum of the horizontal soft layer shear stiffness (Eq. 7), $k2$, and of the soft walls axial stiffness (Eq. 8), $k1$, estimated as being:

$$k_1 \frac{G_g \bullet B}{S_1} \tag{7}$$

$$k_2 = \frac{2 \bullet E_g \bullet H}{S_2} \tag{8}$$

$$K_{barr} = k1 + k2 \tag{9}$$

Equation 9 assumes, by simplifying, that side and base spring reactions are synchronous and that soil around the barriers moved rigidly. As matter of fact, these particularities can be defined as second-order aspects, which are not capable of significantly affect the reliability of the results (Flora et al. 2018).

The damping coefficient of the barriers, C_{barr}, is equal to:

$$C_{barr} = \frac{2k_{barr}\xi_{IS}}{\omega_{IS}} \tag{10}$$

where ξ_{IS} is the equivalent damping mobilized in the barriers and $\omega_{IS} = \frac{2\pi}{T_{is}}$. Regarding the spring that connects the foundation with the superstructure, it is simple to realise that m_{str} is the first modal participating mass of superstructure, while K_{str} is the structural stiffness in a fixed base condition. The foundation soil stiffness is much higher than the stiffness of the barriers, and for this reason the increase in period given by SSI can be neglected. However, if the soil-structure interaction is particularly relevant ($\frac{H_{str}}{V_s T_{FB}} > 0.10$, as suggested by NIST 2012) the value of K_{str} can be reduced by using the theory of the replacement oscillator and a value of K_{eq} can be used (Wolf 1985). The value of C_{str} is equal to:

$$C_{str} = \frac{2k_{str}\xi_{str}}{\omega_{str}} \tag{11}$$

The equations of the coupled horizontal motions suitable for the idealized GSI system can be expressed as follow:

$$m_{IS}\ddot{u}_{IS} + m_{str}\ddot{u}_{str} + C_{bar}\left(\dot{u}_{IS} - \dot{u}_g\right) + K_{barr}\left(u_{IS} - u_g\right) = 0 \tag{12}$$

$$m_{str}\ddot{u}_{str} + C_{str}\left(\dot{u}_{str} - \dot{u}_{IS}\right) + K_{str}\left(u_{str} - u_{IS}\right) = 0 \tag{13}$$

Assuming relative displacements as Lagrangian:

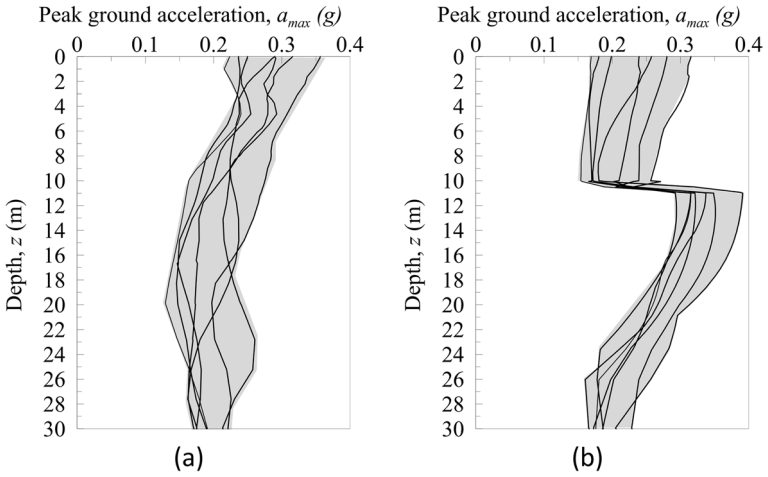

Fig. 19 Maximum PGA profile with depth; **a** without soft barrier intervention, **b** with soft barrier intervention

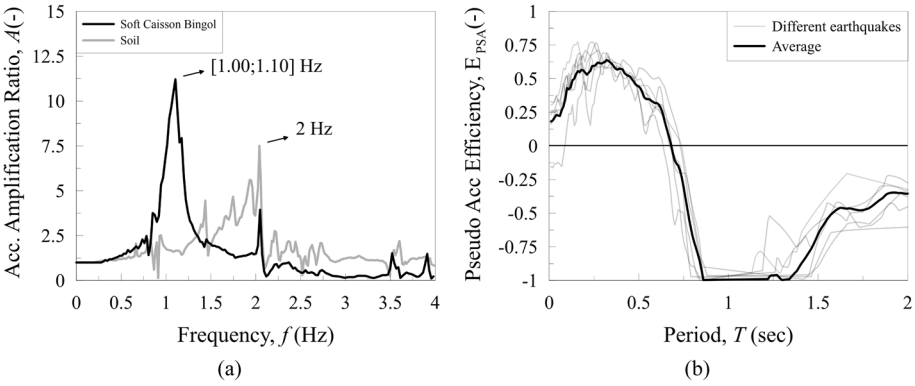

Fig. 20 Acceleration Amplification Function, surface-bedrock (within signal), to detect the resonant period of the soft caisson: **a** Bingol earthquake; **b** efficiency $PSA(T)$ parameter for different natural earthquakes

$$v_{str} = u_{str} - u_{IS} \tag{14}$$

$$v_{IS} = u_{IS} - u_g \tag{15}$$

The equations of motion become:

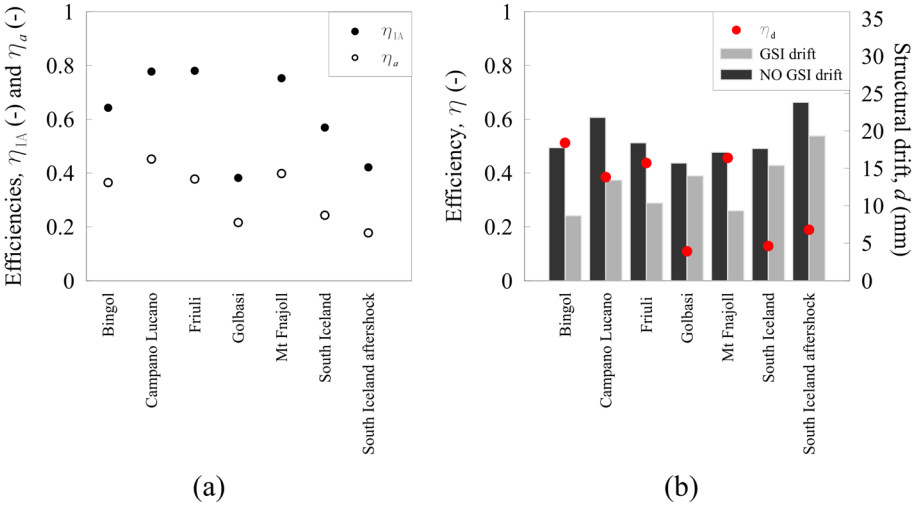

Fig. 21 Efficiency parameters such as: **a** Arias Intensity and Maximum Acceleration Efficiency **b** Maximum Structural Drift and Efficiency in terms of structural displacement reduction

Table 6 Vertical settlements and global rotations of structures

Analysis (–)	NO GSI			GSI		
	δ (m)	β_{max} (rad)	β_{res} (rad)	δ (m)	β_{max} (rad)	β_{res} (rad)
Static	0.0024	–	–	0.0030	–	–
Bingol	0.0180	0.0008	0.0002	0.0059	0.0004	0.0002
Campano Lucano	0.0252	0.0013	0.0010	0.0062	0.0007	0.0003
Friuli	0.0141	0.0009	0.0005	0.0067	0.0004	0.0000
Golbasi	0.0058	0.0007	0.0000	0.0058	0.0007	0.0006
Mt Fnajoll	0.0106	0.0007	0.0004	0.0053	0.0004	0.0001
South Iceland	0.0166	0.0010	0.0004	0.0074	0.0005	0.0004
South Iceland aftershock	0.0195	0.0013	0.0005	0.0101	0.0006	0.0001

$$(m_{IS} + m_{str})\ddot{v}_{IS} + m_{str}\ddot{v}_{str} + C_{barr}\dot{v}_{IS} + K_{barr}v_{IS} = -(m_{str} + m_{IS})\ddot{u}_g \tag{16}$$

$$m_{str}\ddot{v}_{IS} + m_{str}\ddot{v}_{str} + C_{str}\dot{v}_{str} + K_{str}v_{str} = -m_{str}\ddot{u}_g \tag{17}$$

And, in matrix form:

$$[M] \bullet \{\ddot{v}\} + [C]\{\dot{v}\} + [K]\{v\} = -[M][R]\ddot{u}_g \tag{18}$$

With $[R] = [1, 0]^T$, $[v] = \left[v_{IS}, v_{str}\right]^T$.

The system can be solved, step by step, using Newmark's method with a numerical code such as Matlab or Python. In order to validate the DDOF implemented, the parameters reported in Table 7 were selected and the different seismic signal presented in Table 2 were used. Solving the eigenvalue problem for the coupled system of the two previous equations

leads to the evaluation of the two frequencies of the 2DOF system; in this case $f_1 = 1.15$ Hz and $f_2 = 2.63$ Hz. As it is possible to see, the first natural resonance frequency (corresponding to the soft caisson natural resonant frequency) is very close to the soft caisson resonant frequency estimated thought FEM numerical analysis (1.10 Hz, Fig. 22).

The time history accelerations, produced at the centre of gravity of the isolated volume and at the roof of the structure in the numerical FEM analyses, were compared with those produced by the DDOF system (Fig. 23a, b). The comparison between the finite element modelling and the dynamic system modelling results shows substantial agreement (maximum estimated error equal to 15%), suggesting the possibility of using the analytical tool to have a preliminary estimate of the isolating effects of the soft caisson. In particular, this simplified approach will allow the preliminary dimensioning of the caisson system to maximise its anti-seismic effects based on the local hazard conditions and on the peculiar structural properties. Further finite element or finite difference modelling can then be used to refine the design of the soft caisson.

6 Conclusions

The experimental results reported in the first part of this paper allow to better understand the dynamic behavior of SAP-sand mixtures. As expected, the shear waves velocity is reduced as the percentage of SAP in the soil is increased (at the same time, volumetric stiffness increases, thus reducing static concerns, as also discussed by Flora et al. 2015). A new formulation has been proposed to interpret the shear waves velocity as a function of the of SAP percentage and of the effective mean pressure. Furthermore, the influence of the SAP hydration percentage on the SAP-sand dynamic properties was pointed out through a micromechanical possible explanation which can be validated by means of X-ray microtomography. Since for a given amount of SAP its efficiency in both filtering shear waves and increasing damping amplifies as the size of SAP particles decreases, chemical compositions of the polymers not giving rise to extremely large SAP particles should be preferred. This is a relatively simple task, as the properties of SAP can be engineered.

Due to the low shear modulus of the SAP-sand mixtures, the local shear strain level is expected to be very high ($> 1\%$) during earthquakes. Considering also the extremely high values of the damping mobilized at large strains, it can be concluded that SAP-sand mixtures are well suited to be used as bottom horizontal layers of Geotechnical Seismic

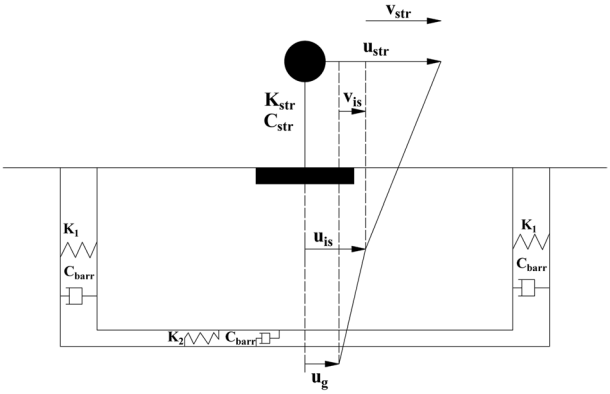

Fig. 22 Dynamic system with two discrete masses and 2 degrees of freedom

Table 7 Parameters of the DDOF system to replicate the numerical analysis

Density of soil, p (kg/m^3)	Structural mass, m_{str} (Mg/m)	Structural stiffness, K_{eq} (kN/m/m)	Dashpot barrier, C_{barr} (kN s/m)	Dashpot structure, C_{barr} (kN s/m)
1566	18.71	5000	695	30

Isolation systems. Incidentally, at high values of SAP content the volumetric stiffness of the SAP-sand mixture increases (as reported for instance by Flora et al. 2015). For this reason, possible settlements or residual tilt of the structure, generated by the soft barriers, are not able to affect the structural stability. Nowadays, since no real scale field test has never been carried out, unfavorable deformations, during the installation of horizontal barriers, cannot be excluded.

The dynamic characterization of these mixtures was used to calibrate a parametric 1D seismic site response analyses using a non-linear material model, considering the effect of a soft layer (SAP80) at different depths. The filtering effect of the barriers confirms to be excellent. Two-dimensional FEM analysis was then carried out highlighting the importance of estimating the natural period of vibration of the soft caisson. Above all, the filtering effect produced by the soft caisson depends on its natural period of vibration. For this reason, the soft caisson must be designed based on the local seismic demand and on the structural dynamic properties. To facilitate this design process, an analytical design models is also described, considering the system of the mass isolated by the soft caisson and the structure on top as a Double Degree Of Freedom (DDOF) system. Comparison with the results of the finite element model shows a margin of error always lower than 15%; for this reason, this tool can be used for a preliminary dimensioning of the soft caisson, immediately indicating if it plays a beneficial role or is detrimental, as it can happen for slender structures.

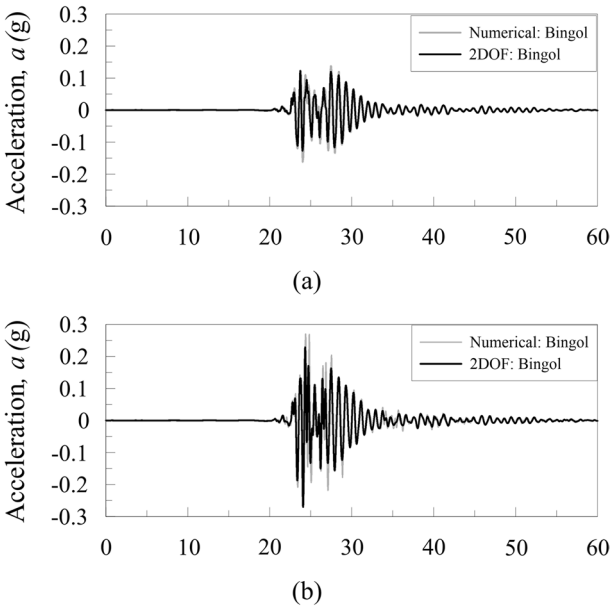

Fig. 23 Comparison between the absolute accelerations: **a** recorded at the centre of gravity of the caisson system with Plaxis 2D and via the dynamic system implemented for Bingol earthquake; **b** at the roof of the structure with Plaxis 2D and via the dynamic system implemented for Bingol earthquake

Acknowledgements The authors would like to show our gratitude to the Tecno In Ltd. for providing the triaxial cell equipped with Bender Element and Post.Doc Lucia Mele for assistance during simple cyclic shear tests. The authors are also very grateful for the contribution made by Eva Cozzolino in the interpretation of dynamic laboratory tests.

Funding The authors declare that no funds, grants, or other support were received during the preparation of this manuscript.

Data availability The datasets generated during the current study are available from the corresponding author on reasonable request.

Declarations

Conflict of interests The authors have no relevant financial or non-financial interests to disclose. All authors contributed to the study conception and design.

References

Airey DW, Wood DM (1986) Pore pressures in simple shear. Soils Found 26(2):91–96
ASTM D5311-11 (2013) Standard test method for load controlled cyclic triaxial strength of soil. ASTM, West Conshohocken
Bjerrum L, Landva A (1966) Direct simple shear tests on a Norwegian quick clay. Geotechnique 16(1):1–20
Brinkgreve RBJ, Swolfs WM, Engine E (2011) PLAXIS user's manual
Charles JA, Skinner HD (2004) Settlement and tilt of low-rise buildings. Proc Inst Civ Eng Geotech Eng 157(GE2):65–75
Flavigny E, Desrues J, Palayer B (1990) Le sable d'Hostun. Rev Fr Géotech 53:67–70
Flora A (2022) 3rd Kerisel Lecture: taking care of heritage, a challenge for geotechnical engineers. In: Third international symposium on geotechnical engineering for the preservation of monuments and historic sites, Naples, Italy, 22–24 June 2022
Flora A, Bilotta E, Lirer S, Nappa V (2015) Soft soil-polymer mixtures for seismic isolation. 6th International Symposium on Deformation Characteristics of Geomaterials, Buenos Aires
Flora A, Lombardi D, Nappa V, Bilotta E (2018) Numerical analyses of the effectiveness of soft barriers into the soil for the mitigation of seismic risk. J Earthq Eng 22(1):63–93
Gatto MPA, Lentini V, Castelli F, Montrasio L, Grassi D (2021) The use of polyurethane injection as a geotechnical seismic isolation method in large-scale applications: a numerical study. Geosciences 11:201
Hardin B, Drnevich V (1972) Shear modulus and damping in soils: measurement and parameter effects. J Soil Mech Found Div ASCE 98(6):603–624
Heron C (2013) The dynamic soil-structure interaction of shallow foundations on dry sand beds. PhD Thesis, University of Cambridge, pp 53–54
Hoque E, Tatsuoka F (2000) Kinematic elasticity of granular material. ISRM International Symposium, Melbourne, Australia
IBC (2018) Italian Building Code: Ministry of Infrastructure and Transport, Rome, Italy
Kirtas E, Pitilakis K (2009) Subsoil interventions effect on structural seismic response. Part II: parametri investigation. J Signal Eng 13(3):328–344
Kirtas E, Rovithis E, Pitilakis K (2009) Subsoil interventions effect on structural seismic response. Part I: validation of numerical simulations. J Signal Eng 13(2):155–169
Kottke AR, Wang X, Rathje EM (2019) Technical manual for strata. Geotechnical Engineering Center, University of Texas, Austin
Kuhlemeyer RL, Lysmer J (1973) Finite element method accuracy for wave propagation problems. J Soil Mech Found Div ASCE 99(SM5):421–427
Kumar SS, Krishna AM, Dey A (2018) Dynamic properties and liquefaction behaviour of cohesive soil in northeast India under staged cyclic loading. J Rock Mech Geotech Eng 10:958–967
Lee J-S, Santamarina JC (2005) Bender elements: performance and signal interpretation. J Geotech Geoenviron Eng 131(9):1063–1070. https://doi.org/10.1061/(asce)1090-0241(2005)131:9(1063)
Mahdavisefat E, Salehzadeh H, Heshmati AA (2018) Full-scale experimental study on screening effectiveness of SRM-filled trench barriers. Géotechnique 68(10):869–882

Matasovic N, Vucetic M (1993) Cyclic characterization of liquefiable sands. J Geotech Eng ASCE 119:1805–1822
Nappa V, Bilotta E, Flora A, Madabhushi G (2016) Centrifuge modelling of the seismic performance of soft buried barriers. Bull Earthq Eng 14:2881–2901
National Institute of Standards and Technology (NIST) (2012) Soil-structure interaction for building structures. Report No. NIST GCR 12-917-21. Prepared for U.S. Department of Commerce, Gaithersburg, MD, US
Pitilakis K, Karapetrou S, Tsagdi K (2015) Numerical investigation of the seismic response of RC buildings on soil replaced with rubber–sand mixtures. Soil Dyn Earthq Eng 79:237–252
Pitilakis D, Anastasiadis A, Vratsikidis A et al (2021) Large-scale field testing of geotechnical seismic isolation of structures using gravel-rubber mixtures. Earthq Eng Struct Dyn 2021(50):2712–2731. https://doi.org/10.1002/eqe.3468
Rathje EM, Abrahamson NA, Bray JD (1998) Simplified frequency content estimates of earthquake ground motions. J Geotech Geoenviron Eng 124(2):150–159
Schanz T, Vermeer P (1998) On the stiffness of sands. Pre-failure deformation behaviour of geomaterials. Thomas Telford, London, pp 383–387
Schanz T, Vermeer P, Bonier P (1999) "Formulation and verification of the Hardening Soil model". Beyond 2000 in Computational Geotechnics. Balkema, Rotterdam
Skempton AW, Macdonald DH (1956) The allowable settlements of buildings. Proc Inst Civ Eng 5(6):727–768
Somma F, Flora A, Bilotta E, Viggiani GM (2021) Numerical analysis on shallow foundations lateral disconnection. In: 8th ECCOMAS thematic conference on computational methods in structural dynamicsand earthquake engineering. Athens, Greece, pp 27–30. https://doi.org/10.7712/120121.8849.19221
Somma F, Bilotta E, Flora A, Viggiani GMB (2022a) Centrifuge modeling of shallow foundation lateral disconnection to reduce seismic vulnerability. J Geotech Geoenviron Eng (ASCE) 148(2):04021187
Somma F, Bilotta E, Flora A, Viggiani GMB (2022b) Lateral disconnection of foundations: a respectful seismic isolation of historic building. In: Geotechnical engineering for the preservation of monuments and historic sites III
Somma F, Lignola G, Ramaglia G, de Sanctis L, Iovino M, Oztoprak S, Flora A (2023) An interdisciplinary approach to interpret earthquake damages to an historic tower and to propose respectful mitigation measures. Bull Earthq Eng. Accepted for publication
Tsang H (2022) Analytical design models for geotechnical seismic isolation systems. Bull Earthq Eng. https://doi.org/10.1007/s10518-022-01469-x
Tsang H, Pitilakis K (2019) Mechanism of geotechnical seismic isolation system: analytical modelling. Soil Dyn Earthq Eng 122:171–184. https://doi.org/10.1016/j.soildyn.2019.03.037
Viggiani G, Atkinson JH (1995) Interpretation of bender element tests. Geotechnique 45(1):149–154
Viggiani C (2017) Geotechnics and Heritage. In: 19th international conference on soil mechanics and geotechnical engineering 17–22 September 2017, Seoul Korea
Wolf JP (1985) Dynamic soil-structure interaction. Prentice Hall, Englewood Cliffs
Xiong W, Li Y (2013) Seismic isolation using granulated tire–soil mixtures for less-developed regions: experimental validation. Earthq Eng Struct Dyn 42:2187–2193
Yegian MK, Catan M (2004) Soil isolation for seismic protection using a smooth synthetic liner. J Geotech Geoenviron Eng 130:1131–1139
Yegian MK, Kadakal U (2004) Foundation isolation for seismic protection using a smooth synthetic liner. J Geotech Geoenviron Eng 130:1121–1130